Supporting Information

Genetically Programmable Microbial Assembly

Mark T. Kozlowski, Bradley R. Silverman, Christopher P. Johnstone, and David A. Tirrell*

Division of Chemistry and Chemical Engineering, California Institute of Technology
Pasadena, California 91125, United States

tirrell@caltech.edu

Table of Contents

Supplemental Materials and Methods

General
Restriction enzymes, ligase, and Q5 DNA polymerase were purchased from New England Biolabs (Beverly, NJ). Nickel NTA was purchased from Qiagen (Hilden, Germany). DNA oligos and G-blocks were purchased from Integrated DNA Technologies (Coralville, IA).

Plasmid Subcloning
Recombinant fusion proteins were produced by standard recombinant DNA technology. DH10b or Mach1 *Escherichia coli* were used for all cloning steps.
Genes encoding soluble Z17 and SpyTag proteins along with elastin solubility/stability tags have been previously cloned by our group into modified pQE-80L plasmids.[1]

Plasmids pKPY680 and pKPY681, which constitutively express mWasabi and mCherry, respectively, were constructed using pmWasabi-N1/pmCherry-C1 as the templates.[2-3] Primers were ordered to amplify mWasabi/mCherry as well as add NsiI-J23100 promoter-SpeI-RBS-MRGS-6xHis to the 5' end of mWasabi/mCherry, and to add HindIII to the 3' end. This fragment was inserted into pBAD33 using NsiI and HindIII sites.

To make the surface-expression constructs, the autotransporter domain downstream of the pelB leader sequence was amplified from pHEA[4] by PCR with the addition of a 5' XhoI and 3' HindIII site to the autotransporter amplicon, which was then digested and inserted into a similarly digested modified pQE-80L plasmid[1] to construct plasmid pAT-Empty. Another G-block was ordered with EcoRI and XhoI sites flanking the T5 promoter, pelB, a 6xHis tag, and the protein of interest (SpyTag, SpyCatcher, SynZip17, SynZip18). These G-blocks were digested with XhoI and HindIII, and inserted into similarly digested pAT-Empty to synthesize plasmids pAT-ST, pAT-SC, pAT-17, and pAT-18 respectively. A schematic of the autotransporter cassette is shown in **Figure S1**.

The autotransporter constructs were also placed under the araBAD promoter to enable tighter control of the aggregation systems. The autotransporter-associative domain fusions from pAT-ST and pAT-SC were PCR amplified and inserted into pBAD33 using Gibson isothermal assembly to synthesize plasmids pBAD-ST and pBAD-SC.

The RBS mutant constructs were obtained from pBAD-ST and pBAD-SC by Quik-Change site-directed mutagenesis to synthesize plasmids pBAD-Low-ST and pBAD-Low-SC respectively.

The arabinose-inducible constructs were also placed in a colE1-origin based plasmid for compatibility with the quorum sensing system. The autotransporter expression operons from pBAD-ST and pBAD-SC (including araBAD promoter and accessory araC gene) were PCR amplified and inserted into pQE-60 using Gibson isothermal assembly to generate pBAT-ST and pBAT-SC.

Plasmid pLuxRI2 was a generous gift from the lab of Frances Arnold. To make plasmid construct pMTK1, we first replaced the pLac/Ara1 promoter in pLuxRI2 with a constitutive pJ23105 promoter. A DNA duplex containing the reverse complement of the pJ23105 promoter, and EcoRI and XhoI sites on the 5' and 3' ends, respectively, was ordered from IDT and inserted into pLuxRI2 following digestion with EcoRI and XhoI. Then the quorum sensing cassette consisting of mWasabi and an additional copy of luxI synthetase under the control of the P_{luxI} promoter, a p15a plasmid origin, and flanking SacI and AvrII sites was synthesized as a gBlock (IDT). Plasmid pLuxRI2 was then digested with SacI and AvrII, allowing for the insertion of the gBlock fragment to form plasmid pMTK1. Variants of the quorum sensing system using a Lux box with the C5A and C16A mutants were synthesized via Quik-Change mutagenesis on pMTK1 to synthesize plasmids pMTK2 and pMTK3 respectively.

Fluorescent proteins were chromosomally integrated using the pOSIP clonetegration system.[5] Genes encoding mWasabi and mCherry under the control of the T5 promoter were PCR amplified and assembled into pOSIP-KO (Addgene #45985). Chemically competent *E. coli* MegaX DH10B T1R cells were mixed with the unpurified assembly reaction and spread on 2xYT agar plates supplemented with 35 mg/L kanamycin sulfate to synthesize strains KY35 and KY36.

Expression of Soluble SynZip and SpyCatcher Proteins

Constructs were transformed into BL21 *E. coli* for expression. Expression was performed in Terrific Broth (12 g/L casein, 24 g/L yeast extract, 0.4% w/v glycerol, 0.017 M monobasic potassium phosphate, 0.072 M dibasic potassium phosphate). Cultures were induced at an optical density at 600nm of 0.6-0.9 to a final concentration of 1 mM isopropyl β-D-1-thiogalactopyranoside (IPTG). Expression was allowed to proceed for 5 h, after which cells were harvested by centrifugation.

For Z17 purification, cultures were resuspended in denaturing lysis buffer (8 M urea, 0.1 M Na_2HPO_4, 10 mM imidazole; pH 8.0), and lysed by sonication. Lysates were cleared by centrifugation and incubated with NiNTA. The resin was washed with lysis buffer followed by wash buffer (8 M urea, 0.1 M Na_2HPO_4, 25 mM imidazole; pH 6.3). Protein was eluted with elution buffer (8 M urea, 0.1 M Na_2HPO_4, 250 mM imidazole; pH 3.5). Purity was confirmed with SDS-PAGE. The protein was then extensively dialyzed against water and lyophilized for storage.

SpyCatcher was purified under native conditions. Cultures were resuspended in native lysis buffer (50 mM NaH_2PO_4, 300 mM NaCl, 10 mM imidazole, 1 mg/mL lysozyme; pH 8.0). Cells were lysed by sonication, and cleared lysates were incubated with NiNTA. The resin was washed with native wash buffer (50 mM NaH_2PO_4, 300 mM NaCl, 25 mM imidazole; pH 8.0) and eluted with native elution buffer (50 mM NaH_2PO_4, 300 mM NaCl, 250 mM imidazole; pH 8.0). Purity was confirmed with SDS-PAGE and purified SpyCatcher was dialyzed against water and lyophilized.

Re-engineering of Quorum Sensing System

In preliminary experiments, we determined that the initial quorum-sensing circuit began turning on at an OD_{600} of approximately 0.4. In order to explore the use of aggregation to turn on the circuit, we reduced the sensitivity of the circuit to AHL by using point mutations identified in Antunes et al.[6] In particular, mutations to the quorum-sensing promoter (Lux box) C5A and C16A were found to shift the quorum-sensing response to higher OD. We confirmed that the C16A mutant remained responsive to AHL (**Figure S5**), and we used this construct for all further experiments.

Dry Cell Mass Measurement

To monitor cell growth during the aggregation process, dry cell masses of bacterial cultures were obtained as functions of time. During aggregation, 10 mL samples were centrifuged at 4000 g for 10 min to pellet cells. Cell pellets were washed with water and then lyophilized to remove residual liquid. The mass of each dry cell fraction was determined on an analytical balance and reported as dry cell mass per volume of culture.

Description and Derivation of Quorum Sensing Model

A model for the quorum sensing genetic circuit in bacterial aggregates was developed from the differential species balance with reaction on the autoinducer. Generically, diffusion of molecules in a dilute, non-convective, reacting system can be written as (Eq S1):[7]

$$\frac{\partial C_A}{\partial t} = D_A \nabla^2 C_A + R_A \#(S1)$$

where C_A is the concentration of the species (here the autoinducer), D_A is the effective diffusion coefficient of the species in the system, ∇^2 is the Laplacian operator, and R_A is the instantaneous rate of generation (or consumption) of the species. Here, we will assume that the rate of generation (production) of the autoinducer can be described as a constant term plus a Hill function to represent the positive feedback in the system (S2). This is a common formalism for transcriptional activation,[8] and has previously been used to characterize the LuxI promoter.[9]

$$R_A = \beta_1 + \beta_2 \frac{C_A^n}{K^n + C_A^n} \#(S2)$$

where β_1 is the zeroth order rate constant for leaky/constitutive expression, β_2 is the rate constant for the Hill function representing transcriptional activation by the autoinducer in positive feedback, and K and n are the Hill function equilibrium constant and coefficient respectively. The full partial differential equation (PDE) that describes reaction-diffusion in the bacterial aggregates is:

$$\frac{\partial C_A}{\partial t} = D_A \nabla^2 C_A + \beta_1 + \beta_2 \frac{C_A^n}{K^n + C_A^n} \#(S3)$$

Next, we consider the boundary and initial conditions of the system. Initially, upon aggregation, we expect that the concentration of the autoinducer will be uniform throughout the aggregate and the bulk, which we will denote as C_{A0}^B. For simplicity, we assume that the aggregates are spheres, with radius R. Then, in order to retain finite concentration, the flux at the center of the sphere (r=0) must be 0. Finally, we write an interfacial mass transport equation that applies at the edge of the sphere. The boundary/initial conditions are written as S4-S6

$$C_A(t = 0, r) = C_{A0}^B \#(S4)$$

$$\frac{\partial C_A(t, r = 0)}{\partial r} = 0 \#(S5)$$

$$D_A \nabla C_A(t, r = R) = k_c\left(C_A^B(t) - C_A(t, r = R)\right) \#(S6)$$

where ∇ is the gradient operator, k_c is the interfacial mass transport coefficient, and $C_A^B(t)$ is the (time-dependent) bulk concentration of autoinducer. To further simplify the boundary condition at the surface, we assume that the mass transport coefficient is large, such that there is negligible interfacial resistance to mass transport. This is reasonable because the aggregates are being vigorously mixed, such that the mass transport resistance is likely to be dominated by the dense network of cells in the aggregate (this corresponds to Biot number>>1). These assumptions, though reasonable for the well-mixed system discussed here, could be relaxed by explicitly considering free medium convection-diffusion and/or interfacial mass transfer (as in Equation S6). Equation S6 then becomes

$$C_A(t,r=R) = C_A^B(t) \ \#(S7)$$

Equations S3-S5 and S7 then are a fully defined PDE inside the aggregate. Before solution, we nondimensionalize as follows:

$$\hat{r} = \frac{r}{R} \ \#(S8)$$

$$\widehat{C_A} = \frac{C_A}{C_{A0}^B} \ \#(S9)$$

$$\hat{t} = \frac{C_{A0}^B}{\beta_1} \ \#(S10)$$

If we rewrite the system with nondimensional variables, we obtain the following:

$$\frac{\partial \widehat{C_A}}{\partial \hat{t}} = \frac{D_A C_{A0}^B}{R^2 \beta_1} \nabla^2 \widehat{C_A} + 1 + \frac{\beta_2 \quad \widehat{C_A}^n}{\beta_1 \left(\frac{K}{C_{A0}^B}\right)^n + \widehat{C_A}^n} \ \#(S11)$$

We will define the following dimensionless parameters:

$$\phi = R\sqrt{\frac{\beta_1}{D_A C_{A0}^B}} \ \#(S12)$$

$$\hat{\beta} = \frac{\beta_2}{\beta_1} \ \#(S13)$$

$$\hat{K} = \frac{K}{C_{A0}^B} \ \#(S14)$$

ϕ is the 0th order Thiele modulus for a sphere,[10] $\hat{\beta}$ represents the ratio of the strength of the activated promoter to constitutive/leaky expression, and $\hat{K}$ represents the equilibrium

constant for the Hill function for the promoter, expressed in units of the initial concentration. The PDE becomes:

$$\frac{\partial \widehat{C_A}}{\partial \hat{t}} = \frac{1}{\phi^2}\nabla^2 \widehat{C_A} + 1 + \hat{\beta}\frac{\widehat{C_A}^n}{\hat{K}^n + \widehat{C_A}^n} \#(S15)$$

$$\widehat{R_A} = \hat{\beta}\frac{\widehat{C_A}^n}{\hat{K}^n + \widehat{C_A}^n} \#(S16)$$

The initial/boundary conditions are now:

$$\widehat{C_A}(\hat{t} = 0,\hat{r}) = 1 \#(S17)$$

$$\frac{\partial \widehat{C_A}(\hat{t},\hat{r} = 0)}{\partial \hat{r}} = 0 \#(S18)$$

$$\widehat{C_A}(\hat{t} = 0,\hat{r}) = \widehat{C_A^B}(t) \#(S19)$$

Finally, we consider $\widehat{C_A^B}(t)$, (i.e. the time evolution of the bulk concentration). The amount of accumulation in the bulk is the total flux through the aggregate surface. Alternatively, it can be calculated as the total amount of autoinducer produced in the aggregate net of the change in the integrated concentration inside the aggregate. Writing this for a discrete time step:

$$\widehat{C_A^B}(\hat{t}) = \widehat{C_A^B}(\hat{t} - \Delta t) + \chi_v(\Delta t \int \widehat{R_A} dV - (\int \widehat{C_A}(\hat{t}) dV - \int \widehat{C_A}(\hat{t} - \Delta t) dV)) \quad \text{(S20)}$$

where integrals are taken over the entire aggregate and χ_v is the volume fraction of the aggregates in solution.

Equations S15-S20 constitute a full mathematical description of the system. In order to solve them for a given parameter set, S15-S19 are first numerically solved for a constant bulk concentration, and then the bulk concentrations as a function of time are solved subject to the solution to the PDE (Equation S20). The PDE is then re-solved, and the two steps are iterated until convergence is reached. We used Matlab's pdepe function for PDE solution.

An ODE describes time evolution of the quorum sensing signal in the bulk in the absence of aggregates. By analogy, we have:

$$\frac{d\widehat{C_A}}{d\hat{t}} = \chi_v\left(1 + \hat{\beta}\frac{\widehat{C_A}^n}{\hat{K}^n + \widehat{C_A}^n}\right) \#(S21)$$

where the volume fraction factor is required to account for dilution into the bulk. Matlab's ode45 function was used for integration. Simulation code can be downloaded with the manuscript.

Table S1: Plasmids used in this study

Name	Backbone/origin/promoter	Purpose
pKY680	pBAD33/p15a/pJ23100	Constitutive expression of mWasabi
pKY681	pBAD33/p15a/pJ23100	Constitutive expression of mCherry
pAT-Empty	pQE80/colE1/T5	Cloning of autotransporter fusion proteins
pAT-17	pQE80/colE1/T5	IPTG-inducible expression of SynZip 17
pAT-18	pQE80/colE1/T5	IPTG-inducible expression of SynZip 18
pAT-ST	pQE80/colE1/T5	IPTG-inducible expression of SpyTag
pAT-SC	pQE80/colE1/T5	IPTG-inducible expression of SpyCatcher
pBAT-ST	pQE60/colE1/araBAD	Arabinose-inducible expression of SpyTag and compatibility with pMTK1-3
pBAT-SC	pQE60/colE1/araBAD	Arabinose-inducible expression of SpyCatcher and compatibility with pMTK1-3
pBAD-ST	pBAD33/p15a/araBAD	Arabinose-inducible expression of SpyTag
pBAD-SC	pBAD33/p15a/araBAD	Arabinose-inducible expression of SpyCatcher
pBAD-Low-ST	pBAD33/p15a/araBAD	Arabinose-inducible expression of SpyTag at a reduced expression level

pBAD-Low-SC	pBAD33/p15a/araBAD	Arabinose-inducible expression of SpyCatcher at a reduced expression level
pMTK1	pHTSUB-105/p15a/luxI	Quorum sensing plasmid with the wild-type Lux Box.
pMTK2	pHTSUB-105/p15a/luxI	Less-sensitive quorum sensing plasmid with the C5A mutation in the Lux Box.
pMTK3	pHTSUB-105/p15a/luxI	Less-sensitive quorum sensing plasmid with the C16A mutation in the Lux Box.

Table S2: Strains used in this study

Name	Genotype	Purpose
KY35	DH10B::P_{T5}-mWasabi	Constitutive expression of mWasabi for cell labeling
KY36	DH10B::P_{T5}-mCherry	Constitutive expression of mCherry for cell labeling
sMTK1	KY36/pMTK3/pAT-ST	Strain capable of quorum sensing and aggregating
sMTK2	KY36/pMTK3/pAT-SC	Strain capable of quorum sensing and aggregating

Table S3: Protein sequences

Protein:	Sequence
Z17 (soluble)	MRGSHHHHHHGSVDGSGSGSGSGSGANEKEELKS KKAELRNRIEQLKQKREQLKQKIANLRKEIEAYKGSG SGSGSGSGALDVPGAGVPGAGVPGEGVPGAGVPG AGVPGAGVPGAGVPGEGVPGAGVPGAGVPGAGVP GAGVPGEGVPGAGVPGAGLDVPGAGVPGAGVPGE GVPGAGVPGAGVPGAGVPGAGVPGEGVPGAGVPG AGVPGAGVPGAGVPGEGVPGAGVPGAGLEHHHHH HKLC
SpyCatcher (soluble)	MRGSHHHHHHGSVDGSGSGSGSGSGAAMVDTLSG LSSEQGQSGDMTIEEDSATHIKFSKRDEDGKELAGA TMELRDSSGKTISTWISDGQVKDFYLYPGKYTFVETA APDGYEVATAITFTVNEQGQVTVNGKATKGDAHIDG SGSGSGSGSGALDVPGAGVPGAGVPGEGVPGAGV PGAGVPGAGVPGAGVPGEGVPGAGVPGAGVPGAG VPGAGVPGEGVPGAGVPGAGLDVPGAGVPGAGVP GEGVPGAGVPGAGVPGAGVPGAGVPGEGVPGAGV PGAGVPGAGVPGAGVPGEGVPGAGVPGAGLEHHH HHHKLC
SpyTag (soluble)	MRGSHHHHHHGSVDAHIVMVDAYKPTKLDVPGAGV PGAGVPGEGVPGAGVPGAGVPGAGVPGAGVPGEG VPGAGVPGAGVPGAGVPGAGVPGEGVPGAGVPGA GLDVPGAGVPGAGVPGEGVPGAGVPGAGVPGAGV PGAGVPGEGVPGAGVPGAGVPGAGVPGAGVPGEG VPGAGVPGAGLEHHHHHHKLN
SpyCatcher-Autotransporter	MKYLLPTAAAGLLLLAAQPAMAMRGSHHHHHHGSV DGAMVDTLSGLSSEQGQSGDMTIEEDSATHIKFSKR DEDGKELAGATMELRDSSGKTISTWISDGQVKDFYL YPGKYTFVETAAPDGYEVATAITFTVNEQGQVTVNG

	KATKGDAHIDLETPTPGPDLNVDNDLRPEAGSYIANL AAANTMFTTRLHERLGNTYYTDMVTGEQKQTTMWM RHEGGHNKWRDGSGQLKTQSNRYVLQLGGDVAQW SQNGSDRWHVGVMAGYGNSDSKTISSRTGYRAKAS VNGYSTGLYATWYADDESRNGAYLDSWAQYSWFD NTVKGDDLQSESYKSKGFTASLEAGYKHKLAEFNGS QGTRNEWYVQPQAQVTWMGVKADKHRESNGTLVH SNGDGNVQTRLGVKTWLKSHHKMDDGKSREFQPFV EVNWLHNSKDFSTSMDGVSVTQDGARNIAEIKTGVE GQLNANLNVWGNVGVQVADRGYNDTSAMVGIKWQ F
SpyTag-Autotransporter	MKYLLPTAAAGLLLLAAQPAMAMRGSHHHHHHGSV DAHIVMVDAYKPTKLDVPGAGVPGAGVPGEGVPGA GVPGAGVPGAGVPGAGVPGEGVPGAGVPGAGVPG AGVPGAGVPGEGVPGAGVPGAGLDVPGAGVPGAG VPGEGVPGAGVPGAGVPGAGVPGAGVPGEGVPGA GVPGAGVPGAGVPGAGVPGEGVPGAGVPGAGLET PTPGPDLNVDNDLRPEAGSYIANLAAANTMFTTRLHE RLGNTYYTDMVTGEQKQTTMWMRHEGGHNKWRD GSGQLKTQSNRYVLQLGGDVAQWSQNGSDRWHVG VMAGYGNSDSKTISSRTGYRAKASVNGYSTGLYAT WYADDESRNGAYLDSWAQYSWFDNTVKGDDLQSE SYKSKGFTASLEAGYKHKLAEFNGSQGTRNEWYVQ PQAQVTWMGVKADKHRESNGTLVHSNGDGNVQTR LGVKTWLKSHHKMDDGKSREFQPFVEVNWLHNSKD FSTSMDGVSVTQDGARNIAEIKTGVEGQLNANLNVW GNVGVQVADRGYNDTSAMVGIKWQF
Z17-Autotransporter	MKYLLPTAAAGLLLLAAQPAMAMRGSHHHHHHGSV DGSGSGSGSGSGSNEKEELKSKKAELRNRIEQLKQK REQLKQKIANLRKEIEAYKGSGSGSGSGSGSLETPTP

	GPDLNVDNDLRPEAGSYIANLAAANTMFTTRLHERL GNTYYTDMVTGEQKQTTMWMRHEGGHNKWRDGS GQLKTQSNRYVLQLGGDVAQWSQNGSDRWHVGVM AGYGNSDSKTISSRTGYRAKASVNGYSTGLYATWYA DDESRNGAYLDSWAQYSWFDNTVKGDDLQSESYKS KGFTASLEAGYKHKLAEFNGSQGTRNEWYVQPQAQ VTWMGVKADKHRESNGTLVHSNGDGNVQTRLGVKT WLKSHHKMDDGKSREFQPFVEVNWLHNSKDFSTSM DGVSVTQDGARNIAEIKTGVEGQLNANLNVWGNVGV QVADRGYNDTSAMVGIKWQF
Z18-Autotransporter	MKYLLPTAAAGLLLLAAQPAMAMRGSHHHHHHGSV DGSGSGSGSGSGSSIAATLENDLARLENENARLEKDI ANLERDLAKLEREEAYFGSGSGSGSGSGSLETPTPG PDLNVDNDLRPEAGSYIANLAAANTMFTTRLHERLG NTYYTDMVTGEQKQTTMWMRHEGGHNKWRDGSG QLKTQSNRYVLQLGGDVAQWSQNGSDRWHVGVMA GYGNSDSKTISSRTGYRAKASVNGYSTGLYATWYAD DESRNGAYLDSWAQYSWFDNTVKGDDLQSESYKSK GFTASLEAGYKHKLAEFNGSQGTRNEWYVQPQAQV TWMGVKADKHRESNGTLVHSNGDGNVQTRLGVKT WLKSHHKMDDGKSREFQPFVEVNWLHNSKDFSTSM DGVSVTQDGARNIAEIKTGVEGQLNANLNVWGNVGV QVADRGYNDTSAMVGIKWQF

Table S4: Engineered ribosome binding site sequences

RBS-Name	RBS Sequence (Putative Shine-Dalgarno sequence in red)	Predicted Strength (% of WT)[a]	Observed Strength (% of WT)[b]
wt-SpyTag	GAGGAGAAATTAACTATG	100	100
low-SpyTag	GAGCGAGAAATTAACTATG	29	25
wt-SpyCat	GAGGAGAAATTAACTATG	100	100
low-SpyCat	GAGCGAGAAATTAACTATG	29	28

[a]RBS strengths were estimated using the Salis Lab RBS calculator (https://salislab.net/software/) [11]

[b]Observed RBS strengths were measured by immunocytochemistry against poly-histidine tags on the N-termini of the displayed proteins followed by flow cytometry.

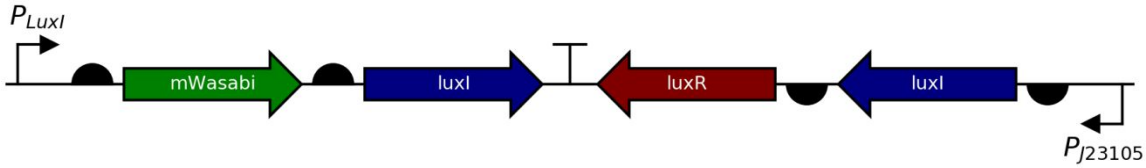

Figure S1: Schematic of quorum-sensing plasmid. On a plasmid with a p15a origin (to ensure compatibility with the aggregation plasmid), luxR activator protein and luxI AHL synthetase are under the control of a pJ23105 constitutive promoter. The LuxR protein, in the presence of a sufficient concentration of AHL, binds to the pLuxI promoter driving expression of mWasabi and an additional copy of luxI AHL synthetase giving rise to positive feedback.

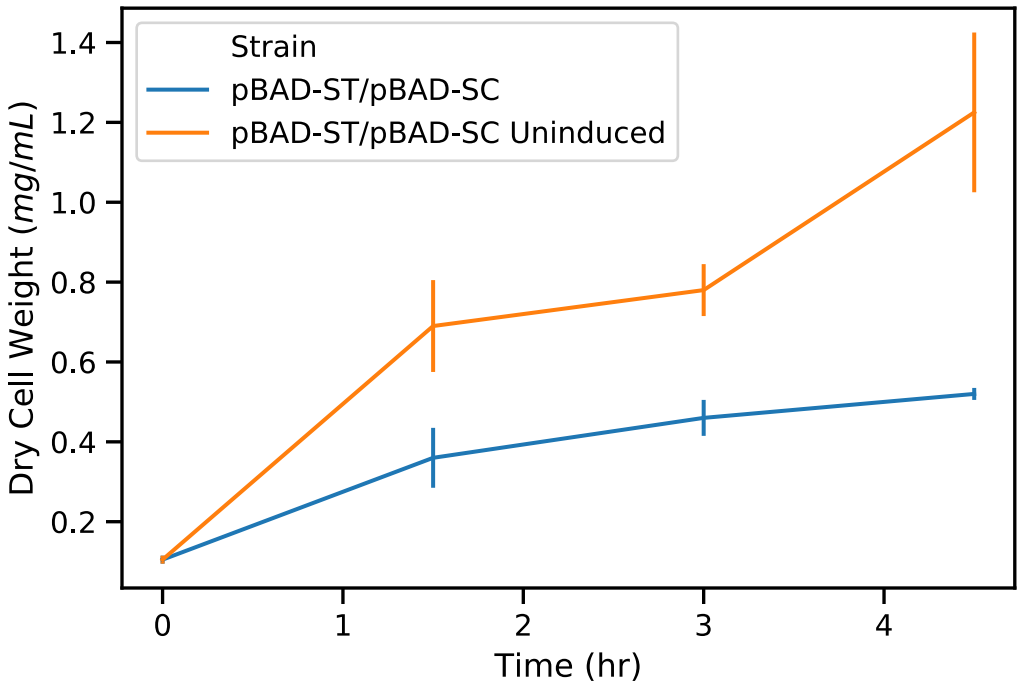

Figure S2: Cell growth during aggregation. Biomass continues to increase during the aggregation process, although not as rapidly as in uninduced cultures. Aggregation was induced at t = 0 by addition of arabinose. Error bars represent SEM (n=2)

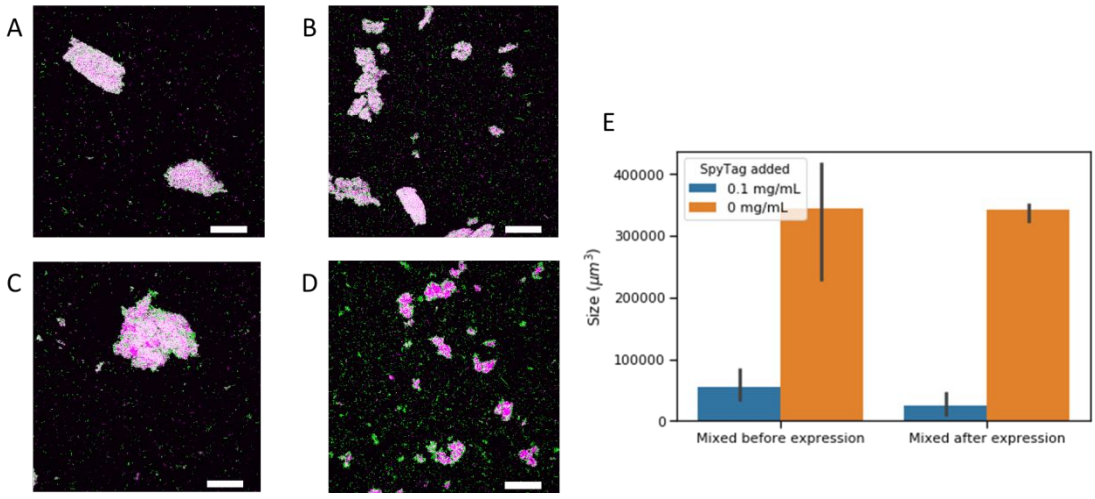

Figure S3: Addition of soluble protein during aggregation of SpyTag (magenta) and SpyCatcher (green) cells. Addition of 0.1 mg/mL soluble SpyTag protein during the aggregation process inhibits the formation of aggregates by forming covalent adducts that block SpyCatcher proteins displayed on the cell surface. **(A-B)** Addition of soluble SpyTag during the mixing of SpyTag and SpyCatcher-displaying bacteria inhibits the formation of very large aggregates, although inhibition is not complete (protein added in B, not in A). **(C-D)** If instead surface display is induced and soluble SpyTag is added prior to mixing of the two strains, then inhibition is more complete (protein added in D, not in C), and aggregates are primarily from non-specific aggregation of SpyTag-displaying bacteria (in magenta). Scale bars in all images represent 100 μm. **(E)** Quantification of aggregate volumes. Volumes after soluble protein addition are significantly smaller in both cases (Error bars represent SEM, n=3, $p<0.05$).

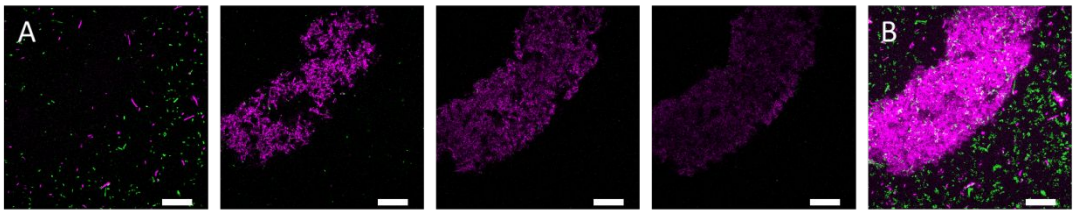

Figure S4: Control core-shell structures. When mWasabi-labeled cells with an empty pBAD-33 plasmid are added to mCherry cores, no shells are formed. **(A)** Z-stack of magnified image of control core-shell structure. Images are shown with 11.6 μm z-spacing with a total thickness of 34.8 μm. Scale bar represents 30 μm. **(B)** Maximum intensity projection of z-stack images shown in (A).

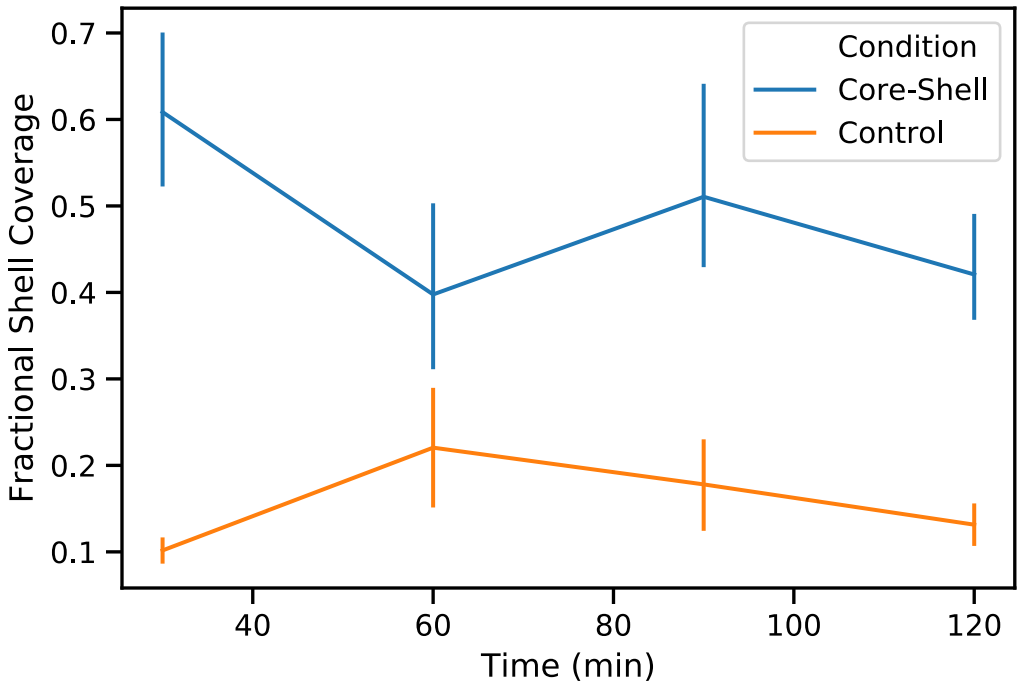

Figure S5: Effect of incubation time on core-shell surface coverage. Though coverage is generally substantially higher when SpyTag is surface displayed, the effect of additional incubation time is small. Surface coverage is expressed as a fraction of mWasabi pixels around the perimeter of the projected area of the aggregate (N=2, error bars represent SEM).

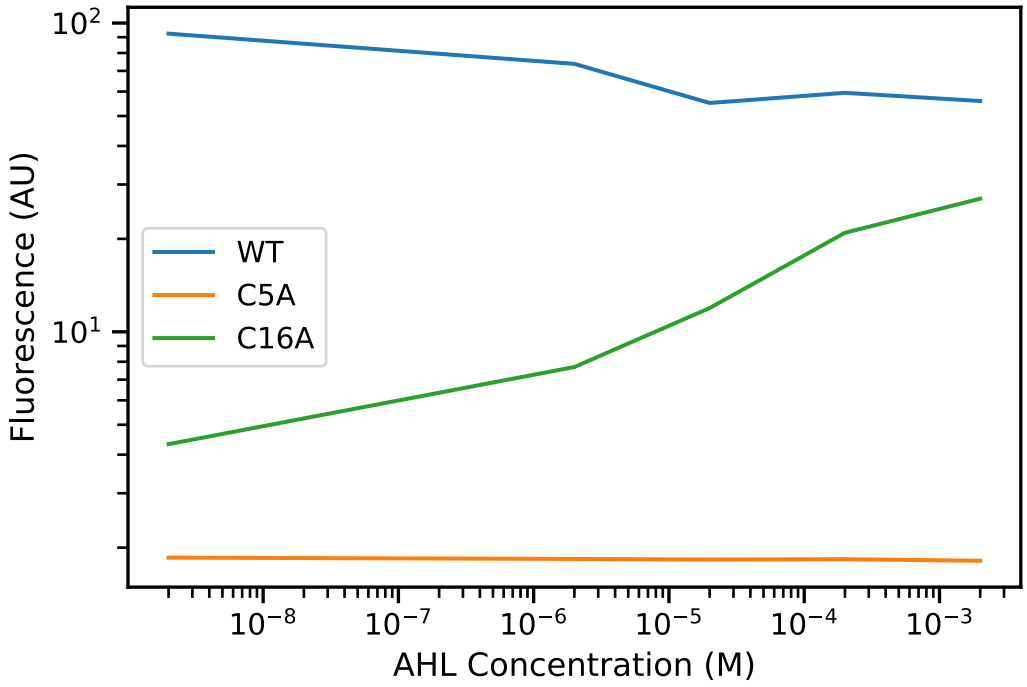

Figure S6: Tuning the sensitivity of the quorum sensing circuit. Endpoint fluorescence measurements for performance of the quorum sensing circuits were obtained as a function of the concentration of exogenous AHL. The C16A mutant, though not the C5A mutant, retains sensitivity to AHL when it is added exogenously. The WT circuit does not show a dose response curve in this setting, as its endogenous production of AHL is sufficient to completely saturate the circuit.

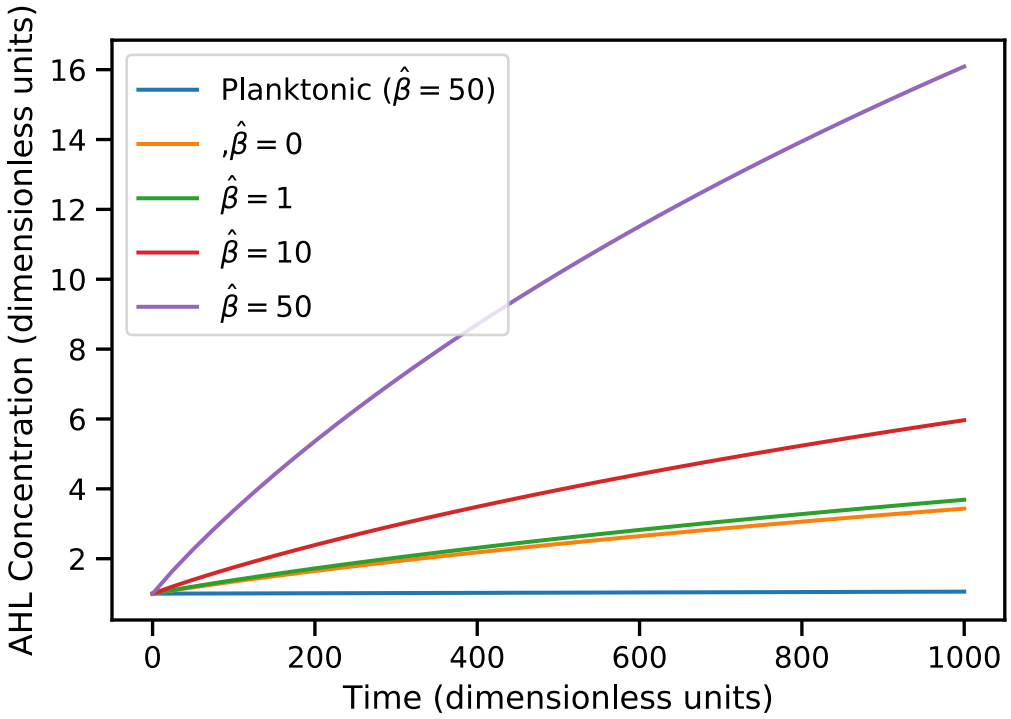

Figure S7: Effect of $\hat{\beta}$ on model. Over a large range of $\hat{\beta}$ (including in its absence, representing no positive feedback), accumulation of autoinducer is much faster than in the unstructured aggregate, which does not accumulate significantly on these time scales. (Other parameters: ϕ=10, $\hat{K}$= 2, n=2)

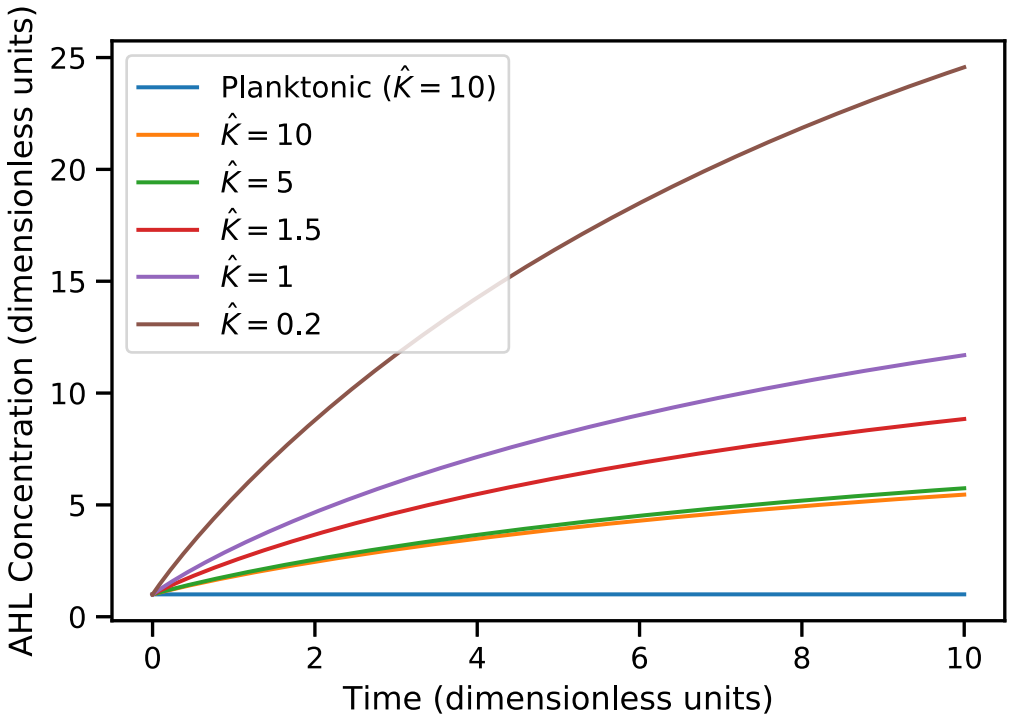

Figure S8: Effect of $\hat{K}$ on model. Over a large range of $\hat{K}$, accumulation of autoinducer is much faster than in the unstructured aggregate, which does not accumulate significantly on these time scales. (Other parameters: ϕ=10, $\hat{B}$=5, n=2)

References

1. Obana, M.; Silverman, B. R.; Tirrell, D. A. Protein-Mediated Colloidal Assembly. *J. Am. Chem. Soc.* **2017**, *139* (40), 14251–14256.

2. Ai, H. W.; Olenych, S. G.; Wong, P.; Davidson, M. W.; Campbell, R. E. Hue-Shifted Monomeric Variants of Clavularia Cyan Fluorescent Protein: Identification of the Molecular Determinants of Color and Applications in Fluorescence Imaging. *BMC Biol.* **2008**, *6* (1), 13.

3. Belin, B. J.; Lee, T.; Mullins, R. D. DNA Damage Induces Nuclear Actin Filament Assembly by Formin-2 and Spire-1/2 That Promotes Efficient DNA Repair. *Elife* **2015**, *4*

4. Veiga, E.; Lorenzo, V. De; Fernandez, L. A. Autotransporters as Scaffolds for Novel Bacterial Adhesins : Surface Properties of Escherichia Coli Cells Displaying Jun / Fos Dimerization Domains. *J. Bacteriol.* **2003**, *185* (18),

5. St-Pierre, F.; Cui, L.; Priest, D. G.; Endy, D.; Dodd, I. B.; Shearwin, K. E. One-Step Cloning and Chromosomal Integration of DNA. *ACS Synth. Biol.* **2013**, *2* (9), 537–541.

6. Antunes, L. C. M.; Ferreira, R. B. R.; Lostroh, C. P.; Greenberg, E. P. A Mutational Analysis Defines Vibrio Fischeri LuxR Binding Sites. *J. Bacteriol.* **2008**, *190* (13), 4392–4397.

7. Deen, W. *Analysis of Transport Phenomena*, 1st ed.; Oxford University Press: New York, 1998.

8. Süel, G. M.; Garcia-Ojalvo, J.; Liberman, L. M.; Elowitz, M. B. An Excitable Gene Regulatory Circuit Induces Transient Cellular Differentiation. *Nature* **2006**, *440* (7083), 545–550.

9. Rai, N.; Anand, R.; Ramkumar, K.; Sreenivasan, V.; Dabholkar, S.;

Venkatesh, K. V.; Thattai, M. Prediction by Promoter Logic in Bacterial Quorum Sensing. *PLoS Comput. Biol.* **2012**, *8* (1).

10. Thiele, E. W. Relation between Catalytic Activity and Size of Particle. *Ind. Eng. Chem.* **1939**, *31* (7), 916–920.

11. Salis, H. M.; Mirsky, E. A.; Voigt, C. A. Automated Design of Synthetic Ribosome Binding Sites to Control Protein Expression. *Nat. Biotechnol.* **2009**, *27* (10), 946–950.